Compact Modeling

Gennady Gildenblat
Editor

Compact Modeling

Principles, Techniques and Applications

Editor
Dr. Gennady Gildenblat
Motorola Professor of Electrical Engineering
Arizona State University
University Drive and Mill Avenue
Tempe, AZ 85287-9309
USA
Gennady.Gildenblat@asu.edu

ISBN 978-90-481-8613-6 e-ISBN 978-90-481-8614-3
DOI 10.1007/978-90-481-8614-3
Springer Dordrecht Heidelberg London New York

Library of Congress Control Number: 2010929773

© Springer Science+Business Media B.V. 2010
No part of this work may be reproduced, stored in a retrieval system, or transmitted in any form or by any means, electronic, mechanical, photocopying, microfilming, recording or otherwise, without written permission from the Publisher, with the exception of any material supplied specifically for the purpose of being entered and executed on a computer system, for exclusive use by the purchaser of the work.

Cover design: eStudio Calamar

Printed on acid-free paper

Springer is part of Springer Science+Business Media (www.springer.com)

Preface

Models of circuit elements which are sufficiently simple to be incorporated in circuit simulators and are sufficiently accurate to make the outcome useful to circuit designers are called compact. The conflicting objectives of model simplicity and accuracy make the compact modeling field an exciting and challenging research area for device physicists, electronic engineers and applied mathematicians. Continued down-scaling of semiconductor devices has made it necessary to incorporate new physical phenomena, while extended applications have led to the inclusion of the secondary and ternary effects in order to achieve the required model accuracy. In addition several rigid requirements in terms of model continuity and qualitative behavior ("benchmarks") have been imposed over the years. At the same time, the increased size of the integrated circuits, that can now be subjected to the full SPICE analysis, disallowed proportional increase in the model execution time. Hence considerable effort went into compact model reformulation in such a way that dramatically increased accuracy and model sophistication are accomplished without prohibitive decrease in the computational efficiency.

The models of MOS transistors underwent revolutionary change in the last few years and are now based on new principles. The recent models of diodes, passive elements, noise sources and bipolar transistors were developed along the more traditional lines. Following this evolutionary development they became highly sophisticated and much more capable to reflect the increased demands of the advanced integrated circuit technology. The latter depends on the compact models for the shortening of the design cycle and eliminating the elements of overdesign which is often undesirable in today's competitive environment. At the same time, statistical modeling of semiconductor devices received new significance following the dramatic reduction of the device dimensions and of the power supply voltage. Finally, despite the complexity of the fabrication process, the multi-gate MOS transistors are now seriously considered for the purpose of controlling the small geometry effects. To evaluate the potential impact of these devices on the IC design, compact models of these devices, preferably based on the same principles as the models of traditional MOSFETs, are becoming important.

The last comprehensive description of the compact models of various semiconductor devices reflects the state of the art in late 1980s [2]. While remaining an in-

fluential and valuable source of information, it can no longer serve the needs of the compact modeling community in the 21st century. In this volume we present contemporary compact models of both active and passive semiconductor devices and discuss general modeling techniques. Given the limited size of the book, and the wide choice of compact models available today, the selection of the topics represented an interesting problem. In the end, it was decided to include compact models which are both heavily used in the industry and at the same time are theoretically significant. For experimental devices like multiple-gate transistors where the optimal choice of the compact models is not yet entirely clear, we have presented two particularly promising approaches. We have also included chapters on the MOSFET noise theory, benchmarking of MOSFET compact models, modeling of the power MOSFET, and overview of the bipolar modeling field. The book concludes with two chapters describing the variability modeling including some recent developments in the field. Once again, since the field of variability modeling is far from maturity, we present several alternative approaches to the subject.

The present volume is comprehensive but is in no way encyclopedic. It does not include several popular and experimental models that have already been described in considerable detail in a book form [1, 5, 6, 8, 11, 13, 15]. Another important subject that is not covered, is the application of behavioral languages in the compact modeling field. Many of the models discussed in this book (e.g. PSP, PSP-SOI, MOSVAR, R3) were developed using verilog-A language which not only significantly reduces the development time, but eliminates numerous potential sources of errors and simplifies model implementation in circuit simulators [10, 12, 14]. Furthermore, we concentrate on the most recent developments in the compact modeling. The reader interested in the evolution of the field can find extensive information in [2, 3, 7, 9] while [4] contains a useful tutorial on compact MOSFET models.

We hope that this volume will be useful to the engineers actively involved in the design of integrated circuits, developing compact models and for the graduate students of the corresponding disciplines.

Arizona State University, Tempe, AZ, USA Gennady Gildenblat

References

1. Aaen, P.H., Plá, J.A., Wood, J.: Modeling and Characterization of RF and Microwave Power FETs. Cambridge University Press, Cambridge (2007)
2. Antognetti, P., Massobrio, G., Massobrio, G.: Semiconductor Device Modeling with SPICE. McGraw-Hill, New York (1993)
3. Arora, N.D.: MOSFET Models for VLSI Circuit Simulation: Theory and Practice. Springer, New York (1993)
4. Bhattacharyya, A.B.: Compact MOSFET Models for VLSI Design. Wiley, New York (2009)
5. Cheng, Y., Hu, C.: MOSFET Modeling and BSIM3 User's Guide. Kluwer Academic, Boston (1999)
6. Enz, C., Vittoz, E.: Charge-Based MOS Transistor Modeling. Wiley, New York (2006)
7. Foty, D.: MOSFET Modeling with SPICE: Principles and Practice. Prentice-Hall, Upper Saddle River (1997)

8. Galup-Montoro, C., Schneider, M.: MOSFET Modeling for Circuit Analysis and Design. World Scientific, Singapore (2007)
9. Graaff, H., Klaassen, F.: Compact Transistor Modelling for Circuit Design. Springer, Berlin (1990)
10. Lemaitre, L., McAndrew, C., Hamm, S.: ADMS: Automated Device Model Synthesize, pp. 27–30 (2002)
11. Liu, W.: MOSFET Models for SPICE Simulation Including BSIM3v3 and BSIM4. Wiley, New York (2001)
12. McAndrew, C.C.: The real barrier to standardized compact models. In: Proceedings of 8th International Conference on Mixed Design of Integrated Circuits and Systems (MIXDES), pp. 53–58 (2001)
13. Miura-Mattausch, M., Mattausc, H.J., Ezaki, T.: The Physics and Modeling of MOSFETs: Surface-Potential Model HiSIM. World Scientific, Singapore (2008)
14. Troyanovsky, B., O'Halloran, P., Mierzwinski, M.: Compact modeling in Verilog-A. In: Grabinski, W., Nauwelaers, B., Schreurs, D. (eds.) Transistor Level Modeling for Analog/RF IC Design, pp. 271–291. Springer, Berlin (2001)
15. Ytterdal, T., Cheng, Y., Fjeldly, T.: Device Modeling for Analog and RF CMOS Circuit Design. Wiley, New York (2003)

Contents

Part I Compact Models of MOS Transistors

1 Surface-Potential-Based Compact Model of Bulk MOSFET 3
Gennady Gildenblat, Weimin Wu, Xin Li, Ronald van Langevelde, Andries J. Scholten, Geert D.J. Smit, and Dirk B.M. Klaassen
1.1 Introduction 3
1.2 Surface Potential Equation 4
1.3 Symmetric Linearization Method 9
1.4 The Effective Channel Mobility 14
1.5 Velocity Saturation 17
1.6 Lateral Doping Non-uniformity 21
1.7 Punch-Through Effect and Vertical Doping Non-uniformity 23
1.8 The Extrinsic Model 27
1.8.1 Overlap Region Charges 27
1.8.2 Parasitic Resistances 28
1.8.3 Impact Ionization Current 29
1.8.4 Gate Tunneling Current 29
1.8.5 Gate-Induced Drain Leakage Current 32
1.9 Surface-Potential-Based Noise Model 32
1.9.1 Flicker Noise 32
1.9.2 Thermal Noise 34
1.9.3 Other Noise Sources 34
1.10 Conclusions 35
References 36

2 PSP-SOI: A Surface-Potential-Based Compact Model of SOI MOSFETs 41
Weimin Wu, Wei Yao, and Gennady Gildenblat
2.1 Introduction 41
2.2 PD-SOI Floating Body Effect Modeling 43
2.2.1 Impact Ionization 45

2.2.2 Junction Diode 45
2.2.3 Parasitic Bipolar Current 46
2.2.4 Gate-to-Body Tunneling Current 48
2.2.5 Gate-Induced Drain Leakage Current 51
2.3 Self-Heating Effect 51
2.4 Body Contact Model 53
2.5 Noise Modeling 57
2.6 PD-SOI MOSFET Model Verification 58
2.7 Modeling of Dynamically Depleted SOI MOSFETs 60
2.7.1 Surface Potential and Coupling Equations 61
2.7.2 Symmetrically Linearized Charge-Sheet Model for DD-SOI 63
2.8 DD-SOI Model Verification and Discussion 67
2.9 Conclusions 70
References 70

3 Benchmark Tests for MOSFET Compact Models 75
Xin Li, Weimin Wu, Gennady Gildenblat, Colin C. McAndrew, and Andries J. Scholten
3.1 Introduction 75
3.2 Benchmark Tests 77
3.2.1 Weak and Moderate Inversion Regions 77
3.2.2 Capacitances 81
3.2.3 Symmetry and Non-Singularity at Zero Drain-Source Bias . 84
3.2.4 Non-Quasi-Static (NQS) and Noise Model Tests 93
3.2.5 Self-Heating Effect Test (SHE) 96
3.3 Conclusion 98
Appendix 1 Derivation of (3.49) and (3.50) 98
Appendix 2 Correlation Coefficient Between Gate and Drain Thermal Noise at $V_{ds} = 0$ 101
References 102

4 High-Voltage MOSFET Modeling 105
E. Seebacher, K. Molnar, W. Posch, B. Senapati, A. Steinmair, and W. Pflanzl
4.1 Introduction 106
4.2 HV LDMOS Modeling with Sub-Circuits 108
4.2.1 HV MOSFET Sub-Circuit Using a Drain Resistor 110
4.2.2 HV MOSFET Sub-Circuit Using a JFET 110
4.2.3 HV MOSFET Sub-Circuit Using Three JFETs 112
4.2.4 HV MOSFET Sub-Circuit Using JFETs, Resistors and Controlled Sources 113
4.2.5 Symmetrical HV MOSFET Sub-Circuit with Bulk Current Modeling 114
4.3 EKV High-Voltage MOSFET Model 115
4.3.1 EKV-HV DC Model 117
4.3.2 EKV-HV Charge Model 118

4.4 MM20 High-Voltage MOSFET Model 119
4.4.1 MM20 DC Model 120
4.4.2 MM20 Charge Model 122
4.5 HiSIM_HV High-Voltage MOSFET Model 123
4.5.1 HiSIM_HV Model Features 123
4.5.2 Resistance Modeling with HiSIM_HV 124
4.5.3 Capacitance Modeling with HiSIM_HV 126
4.6 Modeling of HV MOSFET Parasitics in HV CMOS Technology . . 127
4.6.1 Substrate Based Devices 128
4.6.2 Isolated Devices 130
4.7 Measurement Requirements for HV MOS Modeling 131
4.7.1 DC Measurements for HV MOS Modeling 131
4.7.2 AC Measurements for HV MOS Modeling 131
4.7.3 Pulsed Measurements for HV MOS Modeling 132
References 134

5 Physics of Noise Performance of Nanoscale Bulk MOS Transistors 137
R.P. Jindal
5.1 Introduction 137
5.2 Preliminary Considerations 138
5.3 Intrinsic Fluctuations 139
5.3.1 Channel Thermal Noise 139
5.3.2 Induced Gate Noise 141
5.3.3 Induced Substrate Noise 143
5.3.4 Equilibrium Noise 143
5.3.5 Bulk Charge Effects 144
5.4 Extrinsic Fluctuations 145
5.4.1 Gate Resistance Noise 145
5.4.2 Substrate Resistance Noise 147
5.4.3 Substrate Current Super-Shot Noise 148
5.4.4 Gate Current Noise 150
5.5 Short-Channel Effects 150
5.5.1 Physical Origin 150
5.5.2 Effect On Channel Noise 151
5.5.3 No Excess Noise School of Thought 152
5.5.4 Shot Noise School Of Thought 153
5.5.5 Hot Carrier School of Thought 154
5.6 $1/f$ Noise 155
5.6.1 Number versus Mobility Fluctuations Debate 156
5.6.2 Current Status 156
5.7 Noise Capabilities of Compact MOS Models 157
5.8 Conclusions 158
References 159

Part II Compact Models of Bipolar Junction Transistors

6 Introduction to Bipolar Transistor Modeling 167
Colin C. McAndrew and Marcel Tutt
6.1 Introduction 167
6.2 Basic Bipolar Transistor Operation and Modeling 168
6.3 Base Current 175
6.4 Gummel Integral Charge Control Relation 177
6.5 SPICE Gummel-Poon Model 181
6.6 Small-Signal Model 184
6.7 Kull-Nagel Model 186
6.8 III-V HBTs: Device Physics and Modeling Challenges 189
6.9 Conclusions 195
References 196

7 Mextram 199
R. van der Toorn, J.C.J. Paasschens, W.J. Kloosterman, and H.C. de Graaff
7.1 Introduction 199
7.1.1 History 199
7.1.2 Lumped-Element Modeling 201
7.1.3 Modeling Time-Dependence, Non-Linearity, Large Signals 202
7.1.4 Temperature Dependence and Heating 203
7.1.5 Noise Model 204
7.1.6 Geometric Scaling and Statistical Modeling 204
7.2 Model Structure and Components 205
7.2.1 Outline 205
7.2.2 Relevance of Model Structure to Modeling Results 207
7.3 Mextram Philosophy 216
7.3.1 Introduction 216
7.3.2 Main Transistor Current Model 216
7.4 Conclusion 226
References 227

8 The HiCuM Bipolar Transistor Model 231
Michael Schröter and Bertrand Ardouin
8.1 Introduction 231
8.2 Model Fundamentals 232
8.2.1 Charges 234
8.2.2 Transfer Current 236
8.2.3 Base Current Components 238
8.2.4 Series Resistances 239
8.2.5 NQS Effects 240
8.2.6 Substrate Effects 240
8.2.7 Temperature Effects 241
8.2.8 Noise 241

8.2.9 Geometry Dependence 242
8.2.10 Statistical and Predictive Modelling 243
8.3 Parameter Extraction 244
8.3.1 Parameter Extraction Methods 246
8.4 Application Examples 258
8.5 Conclusions 260
References 263

Part III Compact Models of Passive Devices

9 Integrated Resistor Modeling 271
Colin C. McAndrew
9.1 Introduction 271
9.2 Semiconductor Resistors 273
9.2.1 Effective Resistor Geometry and Total Resistance 274
9.2.2 Resistor Temperature Dependence 276
9.3 2-Terminal Resistor Models 277
9.4 Physical 3-Terminal Resistor Model 278
9.4.1 Diffused Resistor (JFET) Depletion Effect Model 279
9.4.2 Poly Resistor Depletion Effect Model 282
9.4.3 Unified Depletion Effect Model 284
9.4.4 Velocity Saturation 285
9.4.5 Self-Heating 287
9.4.6 Complete 3-Terminal Resistor and JFET Model 288
9.5 Parasitics, Noise and Statistical Modeling 290
9.6 Parameter Extraction 291
9.7 Details of Model Implementation 293
9.8 Conclusions 295
References 296

10 The JUNCAP2 Model for Junction Diodes 299
A.J. Scholten, G.D.J. Smit, R. van Langevelde, and D.B.M. Klaassen
10.1 Introduction 299
10.2 Model Derivation 300
10.2.1 Capacitance 300
10.2.2 Ideal Current 302
10.2.3 Shockley-Read-Hall Current 302
10.2.4 Trap-Assisted Tunneling Current 305
10.2.5 Band-to-Band Tunneling Current 307
10.2.6 Avalanche Breakdown Current 308
10.2.7 Noise 309
10.2.8 Geometrical Scaling 309
10.3 Parameter Extraction 310
10.3.1 Test Structures 310
10.3.2 Extraction of CV Parameters 311
10.3.3 Extraction of IV Parameters 311

10.4 Model Verification 313
10.4.1 Capacitances 313
10.4.2 Currents 313
10.5 JUNCAP2 Express 313
10.6 Model Implementation and Availability 318
10.7 Conclusion 318
Appendix 1 Built-in Voltage 318
Appendix 2 Evaluation of W_{SRH} 320
Appendix 3 Evaluation of W_{Γ} 320
Appendix 4 Evaluation of Γ_{max} 321
Appendix 5 Approximation of the erfc-Function 322
Appendix 6 JUNCAP2 Express 323
References 325

11 Surface-Potential-Based MOS Varactor Model 327
Zeqin Zhu, Gennady Gildenblat, James Victory, and Colin C. McAndrew
11.1 Introduction 327
11.2 Device Technology 328
11.3 Intrinsic Device Model 330
11.4 Inversion Layer Inertia 332
11.4.1 Relaxation Time Approximation 332
11.4.2 Analytical Solution for the Small-Signal Case 333
11.5 The Effects of Finite Polysilicon Doping and Quantum Mechanical Corrections 335
11.6 Gate Tunneling Current 338
11.7 Parasitic Elements 341
11.7.1 Parasitic Capacitance C_{fr} 341
11.7.2 Gate Tunnel Current in the Overlap Region 343
11.7.3 Parasitic Resistances 345
11.8 Silicon Data Validation of RF Model 347
11.9 Circuit Applications Examples 347
11.10 Conclusions 352
References 353

12 Modeling of On-chip RF Passive Components 357
Zhiping Yu
12.1 Introduction 357
12.2 Circuit Requirement and Applications for On-chip RF Passive Components 358
12.3 *R* and *C* Realization in RF CMOS 358
12.3.1 IC Resistors 358
12.3.2 Capacitors in IC Process 360
12.4 Inductors and Transformers 361
12.4.1 Non-planar Inductors: Solenoid 361
12.4.2 Spiral Inductors from Current Sheet 362

12.4.3 CMOS Spiral Inductors 364
12.4.4 Planar Transformers 367
12.4.5 Monolithic Spiral Transformers: Structures 368
12.5 Modeling of Spiral Inductors and Transformers 369
12.5.1 Characterization of Spiral Inductors 369
12.5.2 1-π Model for Spiral Inductors 370
12.5.3 2-π Model for Spiral Inductors 373
12.5.4 Improved 1-π Models for Spiral Inductors 375
12.5.5 Models for Transformers and Baluns 380
12.5.6 Parameter Extraction for Transformer Model 386
12.6 Summary 388
References 390

Part IV Modeling of Multiple Gate MOSFETs

13 Multi-Gate MOSFET Compact Model BSIM-MG 395
Darsen Lu, Chung-Hsun Lin, Ali Niknejad, and Chenming Hu
13.1 Introduction 395
13.1.1 Various Flavors of Multi-gate MOSFET 397
13.1.2 BSIM-IMG and BSIM-CMG 399
13.2 Core Model for the Independent Double-gate MOSFET 399
13.2.1 Basic Modeling Framework 399
13.2.2 Surface Potential Calculation 400
13.2.3 Drain Current Model 404
13.2.4 Capacitance Model 407
13.3 Core Model for the Common Multi-gate MOSFET 409
13.3.1 Basic Modeling Framework 410
13.3.2 Surface Potential Calculation 411
13.3.3 Drain Current Model 413
13.3.4 Capacitance Model 414
13.4 Real Device Effects 415
13.4.1 Quantum Mechanical Effects 415
13.4.2 Short-Channel Effects 417
13.4.3 Effective Width Model 419
13.4.4 Bulk and SOI Substrate Models 419
13.4.5 Other Real Device Effect Models 420
13.5 Experimental Verification 421
13.6 Computational Efficiency 421
13.7 Simulation Examples 424
13.7.1 V_{th} Tuning Simulation for Independent Double-gate MOSFETs 424
13.7.2 FinFET SRAM Technology and Simulation Examples . . 424
13.7.3 Statistical Simulation of FinFET SRAM Cells 425
References 426

14 Compact Modeling of Double-Gate and Nanowire MOSFETs 431
Yuan Taur
14.1 Introduction 431
14.2 Analytic Potential Models for Double-Gate and Nanowire MOSFETs 432
14.2.1 Analytic Solutions to Double-Gate MOSFETs 432
14.2.2 Analytic Solutions to Nanowire MOSFETs 437
14.2.3 Explicit, Continuous Solutions to the Implicit Equations . 438
14.3 Short-Channel Models 440
14.3.1 Short-Channel Model for Double-Gate MOSFETs 440
14.3.2 Short-Channel Model for Nanowire MOSFETs 444
14.4 Charge and Capacitance Models 445
14.5 Discussion of Surface-Potential Based Current Expression 446
14.6 Conclusion 447
References 448

Part V Statistical Modeling

15 Modeling of MOS Matching 453
Marcel Pelgrom, Hans Tuinhout, and Maarten Vertregt
15.1 Introduction 453
15.2 Variability: An Overview 454
15.3 Deterministic Offsets 456
15.3.1 Offset Caused by Electrical Differences 456
15.3.2 Offset Caused by Lithography 457
15.3.3 Proximity Effects 458
15.3.4 Temperature Gradients 460
15.3.5 Offset Caused by Stress 461
15.3.6 Offset Mitigation 464
15.4 Random Matching 466
15.4.1 Random Fluctuations in Devices 466
15.4.2 MOS Threshold Mismatch 469
15.4.3 Current Factor Mismatch 472
15.4.4 Current Mismatch in Strong and Weak Inversion 472
15.4.5 Mismatch for Various Processes 474
15.4.6 Application to Other Components 476
15.4.7 Modeling Remarks 477
15.5 Measuring Offset and Mismatch 477
15.5.1 Matched Pair Test Structures 478
15.5.2 Mismatch Measurement Precision Considerations 479
15.5.3 Statistics for Mismatch Characterizations 480
15.6 Consequences for Design 482
15.6.1 Analog Design 482
15.6.2 Digital Design 484

15.7 Conclusion 485
Appendix: Derivation of Spatial Behavior 485
References 488

16 Statistical Modeling Using Backward Propagation of Variance (BPV) 491
Colin C. McAndrew
16.1 Introduction 491
16.2 Sources of Statistical Variability 492
16.3 Statistical Modeling Basis 495
16.4 Statistical Modeling Requires Engineering Judgment 498
16.5 Modeling Parameter Correlations Using Uncorrelated Parameters 499
16.6 Theoretical Formulation of BPV 502
16.7 BPV Requirements 505
16.8 BPV Application Examples 506
16.9 Corner Models 513
16.10 Why Modeling Correlations is Important 518
16.11 Conclusions 519
References 519

Index 521

Part I
Compact Models of MOS Transistors

Chapter 1
Surface-Potential-Based Compact Model of Bulk MOSFET

Gennady Gildenblat, Weimin Wu, Xin Li, Ronald van Langevelde, Andries J. Scholten, Geert D.J. Smit, and Dirk B.M. Klaassen

Abstract We review surface-potential-based approach to compact modeling of bulk MOS transistors and provide introduction to the widely used PSP model jointly developed by the Arizona State University and NXP Semiconductors. The emphasis is on the interplay between the mathematical structure of the compact model and its capabilities for the circuit design applications.

1.1 Introduction

There is presently a widely held consensus in the industry that the surface-potential-based models represent the best approach to the modeling of bulk and SOI MOS devices. This paradigm change came after careful and deliberate evaluation of different approaches to compact modeling [18, 81] and was enabled by finding innovative solutions for several long-standing problems of compact modeling such as the computationally efficient evaluation of the surface potential and mathematical techniques for incorporating small-geometry effects within the context of the surface-potential-based approach. The motivation for switching from the threshold-voltage-based to surface-potential-based approach comes from the desire to increase the physical content of the compact model and subsequently make it more suitable for modeling advanced MOS devices including low-V_{dd}, analog and RF applications where traditional compact models are not compatible with the circuit design

G. Gildenblat (✉) · W. Wu · X. Li
Ira A. Fulton School of Engineering, Department of Electrical Engineering, Arizona State University, Tempe, AZ 85287, USA
e-mail: gildenblat@asu.edu

R. van Langevelde
Philips Research Europe, 5656 AE Eindhoven, The Netherlands

A.J. Scholten · G.D.J. Smit · D.B.M. Klaassen
NXP-TSMC Research Center, 5656 AE Eindhoven, The Netherlands

G. Gildenblat (ed.), *Compact Modeling*,
DOI 10.1007/978-90-481-8614-3_1, © Springer Science+Business Media B.V. 2010

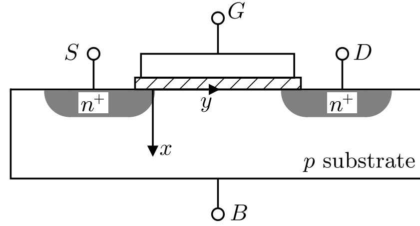

Fig. 1.1 A MOSFET cross-section

requirements in terms of qualitative behavior, $C(V)$ characteristics [36] or model symmetry [3, 31, 67]. The PSP model jointly developed by Arizona State University and NXP is the most advanced MOSFET model incorporating the surface-potential-based approach and has been verified and used in circuit design for the technology nodes from 250 to 32 nm. The description of the early versions of PSP can be found in [68] and [21] in a somewhat condensed form. In this chapter, we provide a more detailed description of the theoretical foundation of PSP, including extension of the symmetric linearization method for all regions of operation and some recent results, such as the origin of the surface potential equation [22], new circuit applications, and modeling of the non-uniformly doped devices. This allows us to examine and illustrate the main features of the surface-potential-based model formulation using PSP as a case study. In what follows, we concentrate on the quasi-static PSP model. The non-quasi-static version is described in [30, 37, 52, 79] and is also surface-potential-based.

1.2 Surface Potential Equation

Surface potential, ψ_s, i.e. the potential at the Si/SiO_2 interface is an implicit function of the terminal voltages that is usually obtained by solving the surface potential equation (SPE) occasionally known also as the input voltage equation. It is derived under several simplifying assumptions essential in the compact model formulation. The first simplification is the Shockley's gradual channel approximation (GCA) that assumes (cf. Fig. 1.1)

$$\left|\frac{\partial^2\psi}{\partial y^2}\right| \ll \left|\frac{\partial^2\psi}{\partial x^2}\right| \tag{1.1}$$

where ψ denotes the electrostatic potential. With this simplification the Poisson equation becomes

$$\frac{\partial^2\psi}{\partial x^2} = -\frac{\rho}{\varepsilon_s} \tag{1.2}$$

where ρ denotes the charge density and ε_s is the dielectric permittivity of silicon. Denoting the electron and hole concentrations as n and p respectively,

$$\rho = q(p - n - N_a^-) \tag{1.3}$$

where N_a^- is the concentration of ionized acceptors and we consider an n-channel MOS device. Since the hole current component is negligible, so is the gradient of the hole imref F_p and the hole concentration is given by the Boltzmann relation $p = p_b \exp(-\beta\psi)$ where $\beta = 1/\phi_t$ and ϕ_t denotes the thermal potential. This form assumes that the reference point for the potential is in the neutral bulk region where the majority and minority carrier concentrations are p_b and n_b respectively. For electrons it is necessary to take into account the imref gradient so that

$$n = n_b \exp[\beta(\psi - \phi_n)] \tag{1.4}$$

where the normalized imref splitting (a.k.a."channel voltage")

$$\phi_n = (1/q)(F_p - F_n). \tag{1.5}$$

For most applications it is sufficient to assume the complete ionization of the channel dopants. Then N_a^- coincides with the total acceptor concentration $N_a = p_b - n_b$ (for the uniformly doped channel). Hence

$$\rho = q\left[p_b\left(e^{-\beta\psi} - 1\right) - n_b\left(ke^{\beta\psi} - 1\right)\right] \tag{1.6}$$

where

$$k = \exp\left(-\beta\phi_n\right). \tag{1.7}$$

From (1.2) and the boundary condition $\partial\psi/\partial x = 0$ for $\psi = 0$ it follows that

$$E_s^2 = -\frac{2}{\varepsilon_s}\int_0^{\psi_s} \rho\, d\psi \tag{1.8}$$

where the surface electric field $E_s = -(d\psi/dx)_{x=0}$. Continuity of the normal component of the displacement vector at the Si/SiO$_2$ interface provides SPE in the form

$$(V_{gb} - V_{fb} - \psi_s)^2 = \gamma^2\phi_t h \tag{1.9}$$

where V_{fb} is the flat-band voltage,

$$\gamma = \sqrt{2q\varepsilon_s p_b}/C_{ox} \tag{1.10}$$

denotes the body factor, unit area oxide capacitance $C_{ox} = \varepsilon_{ox}/t_{ox}$, t_{ox} is the oxide thickness and ε_{ox} is the oxide permittivity. The dimensionless variable h represents the normalized square of the surface electric field:

$$h = \frac{\varepsilon_s E_s^2}{2q\phi_t p_b} = -\frac{1}{q\phi_t p_b}\int_0^{\psi_s} \rho\, d\psi. \tag{1.11}$$

With the exception of the special case of an MOS capacitor where $F_n = F_p$ and $k = 1$, this integral with the charge density (1.6) cannot be obtained in a closed form and further approximations are inevitable in a compact model. The simplest

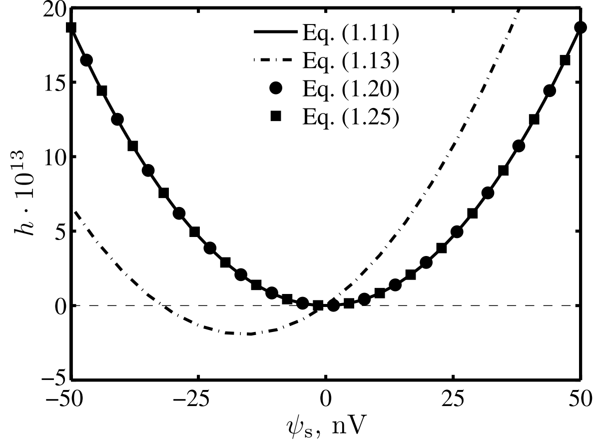

Fig. 1.2 Normalized square of the electrical field as a function of surface potential; $N_a = 2.2 \cdot 10^{17}$ cm^{-3}, $t_{ox} = 2$ nm, and $V_{bs} = 0.47$ V

approximation is obtained by neglecting the position dependence of the electron imref in which case $k = k_0$ where

$$k_0 = \exp(-\beta\phi_{n0}) \tag{1.12}$$

is determined by the imref splitting at the interface. Then $h = h_{PS}$ where [44]

$$h_{PS} = e^{-u} + u - 1 + \frac{n_b}{p_b} k_0 \left(e^u - \frac{u}{k_0} - 1 \right) \tag{1.13}$$

and $u = \beta\psi_s$ is the normalized surface potential. This result reproduced in classic textbooks (e.g. [61]), is exact for MOS capacitors and works well for MOSFETs except for a narrow region near the flat-band (i.e. near $\psi_s = 0$) where h_{PS} becomes negative [40, 83]. This property of (1.13) is incompatible with SPE (1.9) or physical interpretation of h (as the normalized square of the surface electric field) based on (1.11) is illustrated in Fig. 1.2 and can be explained as follows. For $u \to 0$ expansion

$$h_{PS} = (n_b/p_b)(k_0 - 1)u + O(u^2) \tag{1.14}$$

contains a linear term and may become negative if u and $k_0 - 1$ have different signs. As pointed out in [83], the physical origin of this difficulty lies in the assumption $F_n = F_{n0}$, i.e. $\partial\phi_n/\partial x = 0$ made in the derivation of (1.13). In reality, imref splitting ϕ_n is a strong function of both x and y [23, 61] with the standard approximation $\phi_n = \phi_n(y)$ introducing spurious behavior near the flat-band. Despite the fact that the region where $h_{PS} < 0$ is extremely narrow, it may result in the occasional non-convergence of circuit simulations.

We now proceed without assuming $\partial\phi_n/\partial x = 0$. From (1.11)

$$h(u) = e^{-u} + u - 1 + \frac{n_b}{p_b} \left[\int_0^u k(e^w - 1)\,dw + \int_0^u (k-1)\,dw \right]. \tag{1.15}$$

Since the function $e^w - 1$ does not change sign on the interval $(0,u)$ (or $(u,0)$ if $u < 0$), with reference to the first mean value theorem of the integral calculus one has

$$\int_0^u k(e^w - 1)\,dw = k(\xi)\int_0^u (e^w - 1)\,dw; \quad \xi \in (0,u) \tag{1.16}$$

so that [22]

$$h(u) = e^{-u} + u - 1 + \frac{n_b}{p_b}\left[k(\xi)\left(e^u - u - 1\right) + (k_{av} - 1)u\right] \tag{1.17}$$

where

$$k_{av} = \frac{1}{u}\int_0^u k\,dw. \tag{1.18}$$

Comparison with (1.13) shows that h_{PS} is obtained from (1.17) using approximation $k(\xi) = k_{av} = k_0$ which is an immediate consequence of neglecting $\phi_n(x)$ dependence. To improve this result we look for the best approximation of the type $k(\xi) = k_1$ and $k_{av} = k_2$ where coefficients k_1 and k_2 still do not depend on u but are allowed to have different values. Requiring $h(u) = h_{PS}(u)$ in strong inversion region where $h_{PS}(u)$ is physically sound we have $k_1 = k_0$. The second condition

$$h(0) = 0 \quad \text{and} \quad h(u) > 0; \quad u \neq 0 \tag{1.19}$$

implies $k_2 = 1$ whence

$$h = e^{-u} + u - 1 + \frac{n_b}{p_b}k_0\left(e^u - u - 1\right). \tag{1.20}$$

The analysis leading to this result is a variation of that in [22, 40]. It has been recently extended to account for the impurity freeze-out that is essential in low-temperature CMOS applications [22].

The results of the proposed modification of the SPE are shown in Fig. 1.2 illustrating condition (1.19) satisfied by (1.20). Note that apart from the narrow region near $\psi_s = 0$ the difference between (1.13) and (1.20) is small and consequently is invisible to the model user except for eliminating the occasional simulation crash.

Since the SPE (1.9) does not allow for an exact solution, it is solved using either iterative Newton-Raphson procedure [4, 41, 47] or analytical approximations for the surface potential [10, 19–21, 68, 70]. As shown in Fig. 1.3, the approximation used in [10, 84, 85] is particularly accurate leading to the absolute error under 1 nV. As shown in Fig. 1.4, this approximation is sufficiently accurate to evaluate $\Delta\psi$ including the subthreshold region where

$$\Delta\psi \propto \exp(-\beta\psi_{ss})\left[1 - \exp(-\beta V_{ds})\right] \tag{1.21}$$

is exceedingly small [26].

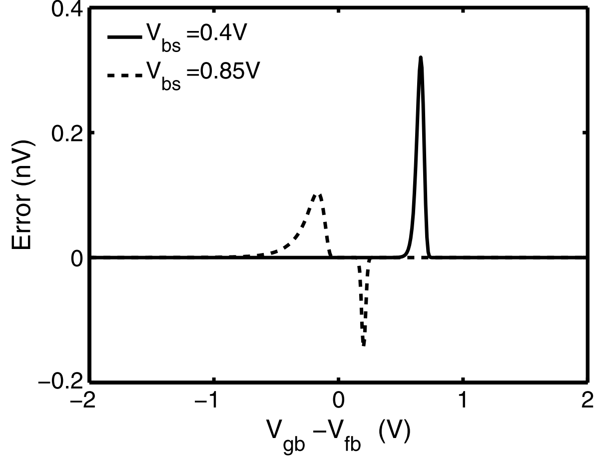

Fig. 1.3 The error in surface potential calculated from analytical approximation relative to the numerical solution for different forward bias; $N_a = 5 \cdot 10^{17}$ cm^{-3}, $t_{ox} = 2$ nm and $T = 300$ K

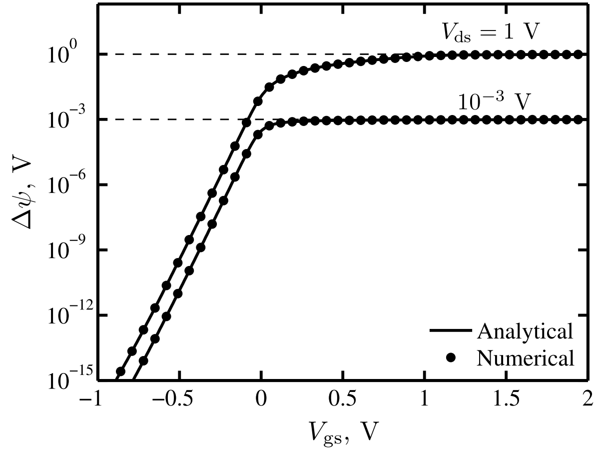

Fig. 1.4 $\Delta\psi$ as a function of the gate bias for various drain-source voltages; $t_{ox} = 2$ nm, $N_a = 10^{17}$ cm^{-3}, $V_{sb} = 0$ V and $T = 300$ K. *Circles* represent the numerical solution of (1.20), while *solid lines* are obtained using analytical approximations for ψ_{ss} and ψ_{sd} [21, 84]

SPE (1.9) with h given by (1.20) implies that derivative

$$\left(\frac{\partial \psi_s}{\partial V_{gb}}\right)_{V_{gb}=V_{fb}} = \frac{1}{1+\gamma\sqrt{(\beta/2)(1+\Delta)}} \tag{1.22}$$

where (ϕ_b denotes the "bulk potential")

$$\Delta = \exp[-\beta(2\phi_b + \phi_n)] \tag{1.23}$$

has different values at the source ($\phi_n = V_{sb}$) and drain ($\phi_n = V_{db}$) ends of the channel. Hence

$$\left(\frac{\partial \Delta\psi}{\partial V_{gb}}\right)_{V_{gb}=V_{fb}} \neq 0 \tag{1.24}$$

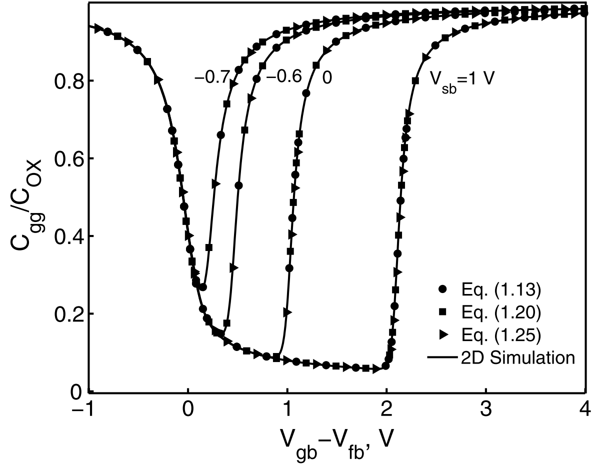

Fig. 1.5 Normalized capacitances computed using (1.13), (1.20) and (1.25). After [83]

where $\Delta\psi = \psi_{sd} - \psi_{ss}$ is the surface potential variation across the channel. This makes it impossible to simplify the model by setting $\Delta\psi = 0$ in accumulation region where $\Delta\psi$ is negligible.

To achieve this simplification in the PSP model h is selected in the form [84]

$$h = e^{-u} + u - 1 + \frac{n_b}{p_b} k_0 \left(e^u - u - 1 - \frac{u^2}{u^2 + 1} \right). \tag{1.25}$$

With this modification, condition (1.19) remains in place but the derivative

$$\left(\frac{\partial \psi_s}{\partial V_{gb}} \right)_{V_{gb}=V_{fb}} = \frac{1}{1 + \gamma\sqrt{\beta/2}} \tag{1.26}$$

does not depend on Δ and remains the same at both ends of the channel enabling approximation $\Delta\psi = 0$ for $V_{gb} < V_{fb}$. As shown in Fig. 1.5 the difference between (1.20) and (1.25) does not affect the device output characteristics and is a matter of convenience.

1.3 Symmetric Linearization Method

All compact surface-potential-based MOSFET models are based on the charge-sheet approximation [5, 64] justified by comparison with the Pao-Sah double integration formula [44]. Since the expressions for current and especially for the terminal charges in Brews' model are quite complicated [40, 77] they need to be simplified before implementation in the compact models [20, 21, 74]. Symmetric linearization method (SLM) developed in [11, 77] (also mentioned in [73]) represents a systematic way to address this problem. The original work in [11, 77] and its subsequent exposition [21, 68] deal with a simplified formulation applicable when the surface

potential satisfies inequality $\psi_s > 3\phi_t$ excluding flat-band condition and accumulation region essential in the formulation of the complete model. In this section, we present SLM in a more complete form which is actually used in the formulation of the SP and PSP models [20, 21].

For this purpose, we introduce the inversion, q_i and bulk, q_b charges per unit area normalized to unit area oxide capacitance. Charge neutrality implies

$$q_i = -(V_{gb} - V_{fb} - \psi_s) - q_b \tag{1.27}$$

where we used the physical signs for q_i and q_b. In its usual form the charge-sheet approximation assumes that depletion theory expression

$$q_b = -\gamma\sqrt{\psi_s - \phi_t}; \quad \psi_s > 3\phi_t \tag{1.28}$$

remains valid even after the formation of the inversion layer [5, 64]. To remove the $\psi_s > 3\phi_t$ limitation, the expression for q_b can be modified as follows [81]:

$$q_b = -\gamma\sqrt{\psi_s - \phi_t[1-\exp(-u)]} \cdot \mathrm{sgn}(\psi_s) \tag{1.29}$$

where the term $\phi_t \exp(-u)$ accounts for the majority carrier contribution and assures that the argument of the square root in (1.29) is non-negative.

In what follows, it is convenient to introduce functions

$$P(u) = e^{-u} + u - 1 \tag{1.30}$$

$$D(u) = \Delta(\phi_n)[e^u - u - 1 - \chi(u)] \tag{1.31}$$

where

$$\Delta(\phi_n) = \exp[-\beta(2\phi_b + \phi_n)] \tag{1.32}$$

and normalized body factor $G = \gamma\sqrt{\beta}$. Then SPE (1.9) becomes

$$[\beta(V_{gb} - V_{fb}) - u]^2 = G^2[P(u) + D(u)]. \tag{1.33}$$

Then $q_b = -\phi_t G\sqrt{P}$ and from (1.28) and (1.33)

$$q_i = -\frac{\phi_t G D(u)}{\sqrt{P(u) + D(u)} + \sqrt{P(u)}}. \tag{1.34}$$

To develop SLM we also introduce the average surface potential

$$\psi_m = \frac{1}{2}(\psi_{ss} + \psi_{sd}) \tag{1.35}$$

and call the point in the channel where $\psi_s = \psi_m$ "the surface potential midpoint". The values of u, q_i, D and P at the surface potential midpoint are denoted as u_m, q_{im}, D_m and P_m respectively.

The main approximation of the symmetric linearization method is [11]

$$q_i = q_{im} + \alpha \cdot s \tag{1.36}$$

where

$$s = \psi_s - \psi_m \tag{1.37}$$

and

$$\alpha = \left(\frac{dq_i}{d\psi_s}\right)_{\psi_s=\psi_m}. \tag{1.38}$$

From (1.27) and (1.29)

$$\alpha = 1 - \left(\frac{dq_b}{d\psi_s}\right)_{\psi_s=\psi_m} = 1 + \frac{G(1-e^{-u_m})}{2\sqrt{P_m}}. \tag{1.39}$$

To use expression (1.34) for q_{im} it is first necessary to obtain D_m which can be done by manipulating SPE (1.33) at the source and drain ends of the channel where the values of imref splitting ϕ_n are known. This yields

$$D_m = \frac{D_s + D_d}{2} + \frac{P_s + P_d}{2} - P_m - \frac{\varphi^2}{4G^2} \tag{1.40}$$

where $D_s = D(\beta\psi_{ss})$, $D_d = D(\beta\psi_{sd})$, P_s and P_d are similarly defined and $\varphi = \beta\Delta\psi$. Using (1.30)

$$D_m = \frac{D_s + D_d}{2} + e^{-u_m}\left(\cosh\frac{\varphi}{2} - 1\right) - \frac{\varphi^2}{4G^2}. \tag{1.41}$$

Since either the second term is negligible or $\varphi \ll 1$ (in subthreshold) it is safe to make approximation

$$\cosh\frac{\varphi}{2} \approx 1 + \frac{\varphi^2}{8} \tag{1.42}$$

so that finally

$$D_m = \frac{D_s + D_d}{2} + \left(e^{-u_m} - \frac{2}{G^2}\right)\frac{\varphi^2}{8} \tag{1.43}$$

which is the form used in SP and PSP models.

Combining (1.36) with the standard expression of the charge-sheet model [5, 64]

$$I_d = -\mu W C_{ox}\left(q_i\frac{d\psi_s}{dy} - \phi_t\frac{dq_i}{dy}\right) \tag{1.44}$$

one finds

$$I_d = -\mu W C_{ox}\left(q_{im} + \alpha \cdot s - \alpha\phi_t\right)\frac{ds}{dy}. \tag{1.45}$$

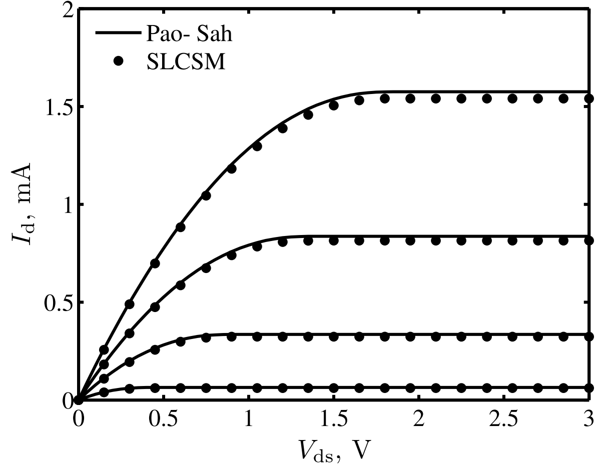

Fig. 1.6 Comparison of $I(V)$ characteristics for Pao-Sah and SLCSM models; $N_a = 2 \cdot 10^{17}$ cm^{-3}, $t_{ox} = 2$ nm and $W/L = 10/10$ µm

Here μ denotes the effective channel mobility while W and L are the width and length of the device, respectively. Separating variables and integrating yields expression for the drain current in the form

$$I_d = \mu \frac{W}{L} C_{ox} \left(-q_{im} + \alpha\phi_t\right) \Delta\psi \tag{1.46}$$

where $\Delta\psi = \psi_{sd} - \psi_{ss}$ is the surface potential variation along the channel. The accuracy of this result is demonstrated by comparison with the Pao-Sah model shown in Fig. 1.6 where abbreviation SLCSM stands for symmetrically-linearized charge-sheet-model.

Since in the rectangular channel device I_d is position-independent, (1.45) can be regarded as a differential equation for the surface potential (or, equivalently, s) as a function of position, y. From (1.45) and (1.46)

$$\frac{dy}{ds} = \frac{L(H-s)}{H\Delta\psi} \tag{1.47}$$

where $H = H_0$ and

$$H_0 = -\frac{q_{im}}{\alpha} + \phi_t. \tag{1.48}$$

After integration

$$y = y_m + \frac{Ls}{H\Delta\psi}\left(H - \frac{s}{2}\right) \tag{1.49}$$

where y_m denotes the coordinate of the "surface potential midpoint" where $\psi_s = \psi_m$. To find y_m note that $s = -\Delta\psi/2$ for $y = 0$ whence

$$y_m = \frac{L}{2}\left(1 + \frac{\Delta\psi}{4H}\right). \tag{1.50}$$

Unlike the case of the complete CSM [77] not only $y(\psi_s)$ but also $\psi_s(y)$ dependence becomes available in a closed form. Indeed, from (1.49) it follows that

$$\psi_s = \psi_m + H\left[1 - \sqrt{1 - (2\Delta\psi/HL)(y - y_m)}\right]. \tag{1.51}$$

The accuracy of this result has been demonstrated in [77].

To insure charge conservation, modern MOSFET models are charge-based with transcapacitances

$$C_{ij} = (2\delta_{ij} - 1)\frac{\partial Q_i}{\partial V_j} \tag{1.52}$$

provided directly by the circuit simulators. In (1.52) $i, j \in \{g, s, d, b\}$ and δ_{ij} denotes the "Kronecker" delta. The physical meaning of the terminal charges

$$Q_g = WC_{ox}\int_0^L (V_{gb} - V_{fb} - \psi_s)\,dy \tag{1.53}$$

and

$$Q_b = WC_{ox}\int_0^L q_b\,dy \tag{1.54}$$

is clear, however, the partition of the inversion charge $Q_i = -Q_g - Q_b$ into the source Q_s and drain $Q_d = Q_i - Q_s$ components requires a few comments. Commonly used Ward-Dutton partition [80]

$$Q_d = WC_{ox}\int_0^L (y/L)q_i\,dy \tag{1.55}$$

is appropriate for uniformly doped channels but not in general [1, 14]. Since in advanced MOSFETs lateral channel non-uniformity is essential (e.g. HALO doping [6]) Ward-Dutton partition should be regarded as an approximation. Numerical studies have shown that while the error introduced by (1.55) is noticeable, it does not at present justify switching back to capacitance-based modeling for circuit simulations.

Symmetric linearization method allows one to obtain simple closed form expressions for the terminal charges. For example, with reference to (1.47) and (1.49)

$$\frac{Q_d}{WLC_{ox}} = \frac{1}{H\Delta\psi}\int_{-\Delta\psi/2}^{\Delta\psi/2}\left[\frac{y_m}{L} + \frac{s(H - \frac{s}{2})}{H\Delta\psi}\right](q_{im} + \alpha s)(H - s)\,ds. \tag{1.56}$$

After integration

$$\frac{Q_d}{WLC_{ox}} = q_{im} + \frac{\alpha\Delta\psi}{12}\left(1 - \frac{\Delta\psi}{2H} - \frac{\Delta\psi^2}{20H^2}\right) \tag{1.57}$$

where the physical signs have been retained for both q_{im} and Q_d. Similarly,

$$\frac{Q_g}{WLC_{ox}} = V_{oxm} + \frac{\Delta\psi^2}{12H} \tag{1.58}$$

and

$$\frac{Q_i}{WLC_{ox}} = q_{im} + \frac{\alpha\Delta\psi^2}{12H} \tag{1.59}$$

where $V_{oxm} = V_{gb} - V_{fb} - \psi_m$ denotes the oxide voltage at the surface potential midpoint. In the SP and PSP models these expressions are used for $V_{gb} > V_{fb}$. As explained above for $V_{gb} \leq V_{fb}$ it is safe to set $\Delta\psi = 0$ so that $Q_g = WLC_{ox}V_{oxm}$ while $Q_s = Q_d = 0$ and $Q_b = -Q_g$. Since I_d is also negligible for $V_{gb} \leq V_{fb}$, this eliminates the need to evaluate the linearization coefficient α in the accumulation region.

As has been done with the expression (1.46) for the drain current, the accuracy of the symmetric linearization method application to the terminal charges has been verified by comparison with Pao-Sah model. Typical results are shown in Fig. 1.7. In addition for $\psi_{ss} > 3\phi_t$ one can also compare the results of the symmetric linearization method with conventional charge-sheet model. This has been done in [11, 68, 77].

To simplify the exposition of the symmetric linearization method we have neglected two important phenomena affecting the MOSFET performance: the quantum corrections and the effect of the polysilicon depletion layer. Both of these effects are included in PSP essentially as discussed in [17] and [74]. The presentation of symmetric linearization method without the assumption of the complete ionization of acceptors can be found in [22].

1.4 The Effective Channel Mobility

The effective channel mobility μ in the MOSFET channel is reduced relative to the bulk mobility as a result of the changed electron-phonon interaction, surface roughness scattering and increased Coulomb scattering. In the engineering models of the transistors these effects are usually combined via Matthiessen's rule to obtain semi-empirical expressions. The model used in PSP is as follows

$$\mu = \frac{\mathbf{UO} \cdot \mu_x}{1 + (\mathbf{MUE} \cdot E_{eff})^{\mathbf{THEMU}} + \mathbf{CS} \cdot [q_{bm}/(q_{bm} + q_{im})^2] + G_R} \tag{1.60}$$

where **UO** is the model parameter roughly corresponding to the low-field mobility (at this point we only discuss the effects of the vertical field), parameters **MUE** and **THEMU** describe effective mobility reduction by the effective vertical field E_{eff}, **CS** is the model parameter introducing the Coulomb scattering following [27] and G_R accounts for the series resistance. PSP also allows for the introduction of the source and drain series resistances directly (using extra nodes that are collapsed by

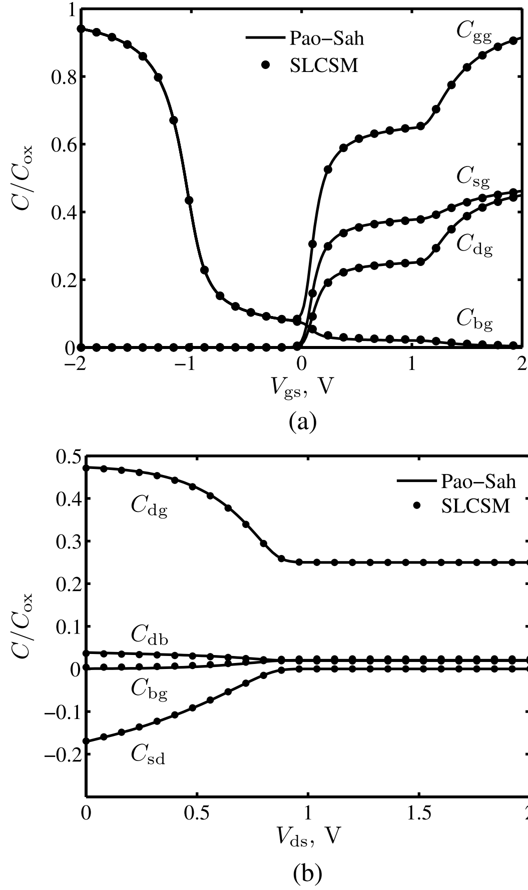

Fig. 1.7 Comparison of $C(V)$ characteristics for Pao-Sah and SLCSM models; $N_a = 2 \cdot 10^{17}$ cm^{-3}, $t_{ox} = 2$ nm, $V_{sb} = 0$, in (**a**) $V_{ds} = 1$ V and in (**b**) $V_{gs} = 1$ V

default) in which case $G_R = 0$. If G_R is used source and drain series resistances R_s are assumed to be equal and

$$G_R = \mathbf{UO} \cdot (W/L) \cdot q_{im} \cdot R_s. \tag{1.61}$$

The effective lateral field is usually defined as

$$E_{eff} = \frac{q_{bm} + \eta_\mu \cdot q_{im}}{\varepsilon_{\rm Si}} \tag{1.62}$$

with $\eta_\mu = 1/2$ for the n-channel [49] and $\eta_\mu = 1/3$ for the p-channel [2] devices. Since, generally speaking, η varies with technology, PSP allows one to adjust η using parameter **FETA** with the default value of 1:

$$\eta_\mu = \begin{cases} \mathbf{FETA}/2 & \text{for NMOS,} \\ \mathbf{FETA}/3 & \text{for PMOS.} \end{cases} \tag{1.63}$$

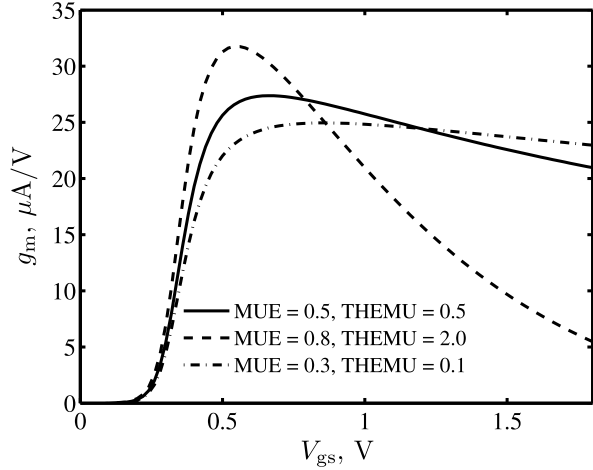

Fig. 1.8 Linear transconductance for different values of mobility model parameters; $V_{ds} = 50$ mV

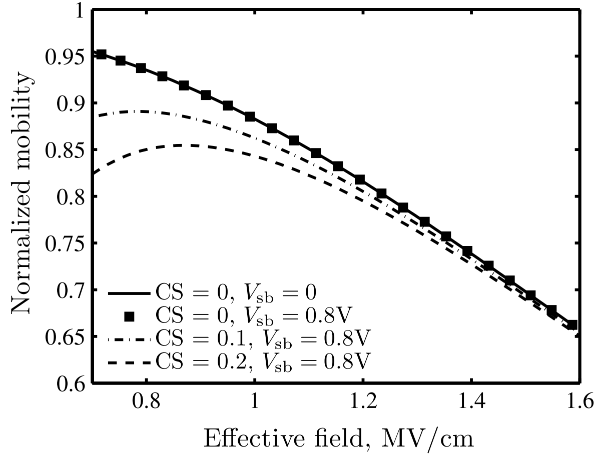

Fig. 1.9 Normalized channel mobility as a function of electrical field; $V_{ds} = 50$ mV

Strictly speaking, the effective channel mobility varies across the MOSFET channel as a result of the position dependence of E_{eff}, q_i, q_b and some other factors (e.g. doping level). While in principle it is possible to include such dependence explicitly, the resulting model complication is not warranted in the compact model. For this reason all variables affecting the effective channel mobility are evaluated at the surface potential midpoint to assure the Gummel symmetry of the model.

Typical results are shown in Fig. 1.8. By changing parameters **MUE** and **THEMU** one can control both the magnitude and the functional dependence of the mobility degradation by the vertical field. In the absence of the Coulomb scattering PSP mobility model is “universal”. The introduction of the Coulomb scattering further reduces the effective mobility and introduces the non-universality effects, especially close to threshold and in the subthreshold region (cf. Fig. 1.9). Additional non-universality effects are described by the function μ_x ($\mu_x = 1$ for the default pa-